iScience

CellPress
OPEN ACCESS

Article

Presenilin-1 in smooth muscle cells facilitates hypermuscularization in elastin aortopathy

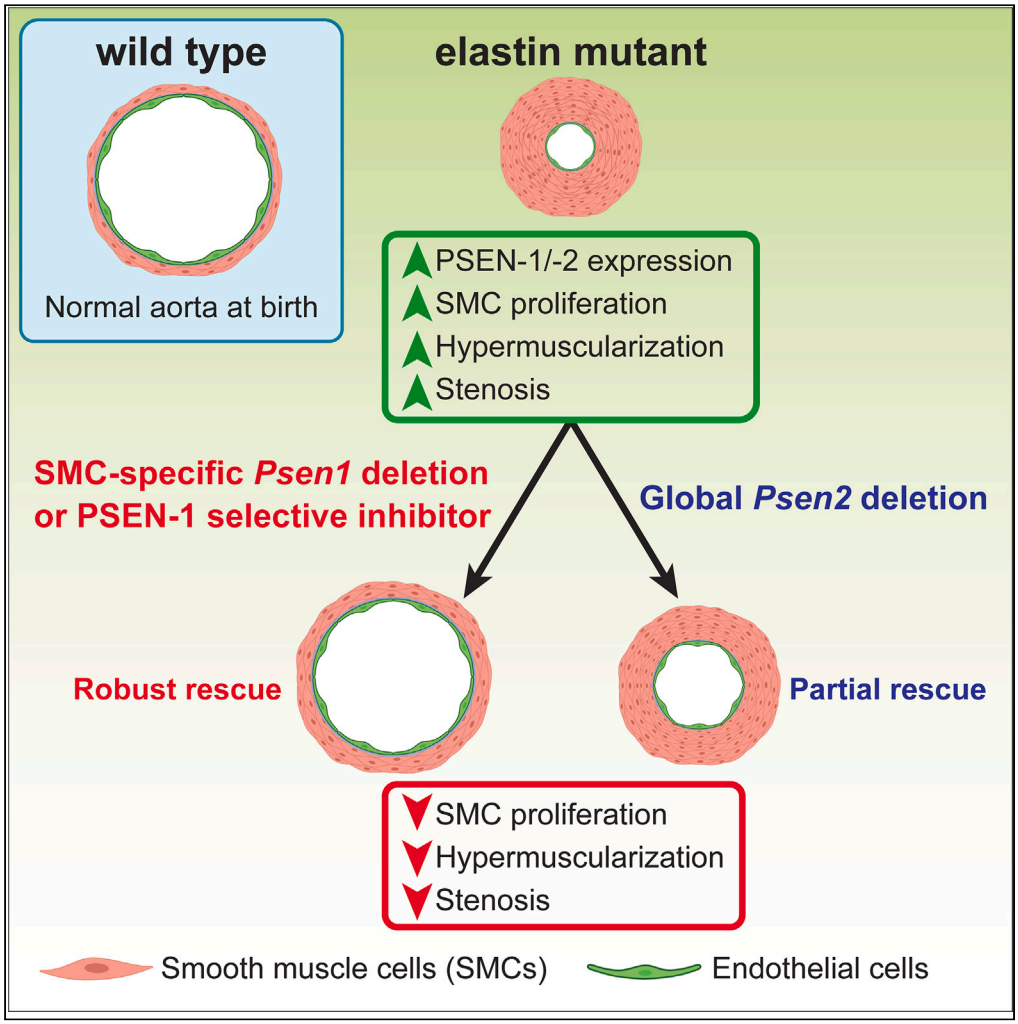

Junichi Saito, Jui M. Dave, Freddy Duarte Lau, Daniel M. Greif

daniel.greif@yale.edu

Highlights

Elastin insufficiency in smooth muscle cells (SMCs) upregulates presenilin (PSEN)

Deletion of either Psen1 in SMCs or Psen2 globally attenuates elastin aortopathy

Among subunits and vascular cell types, SMC Psen1 deletion rescues most robustly

PSEN-1 inhibitor reduces SMC accumulation and stenosis in elastin mutant aorta

Saito et al., iScience *27*, 108636
January 19, 2024
https://doi.org/10.1016/j.isci.2023.108636

iScience

CellPress
OPEN ACCESS

Article

Presenilin-1 in smooth muscle cells facilitates hypermuscularization in elastin aortopathy

Junichi Saito,[1,2,3] Jui M. Dave,[1,2,3] Freddy Duarte Lau,[1,2] and Daniel M. Greif[1,2,3,4,*]

SUMMARY

Smooth muscle cell (SMC) accumulation is central to the pathogenesis of elastin-defective arterial diseases, including supravalvular aortic stenosis (SVAS). We previously demonstrated that elastin insufficiency activates Notch signaling in aortic SMCs. Activation of Notch is catalyzed by the enzyme gamma-secretase, but the role of catalytic subunits presenilin (PSEN)-1 or PSEN-2 in elastin aortopathy is not defined. Genetic approaches reveal that endothelial cell-specific *Psen1* deletion does not improve elastin aortopathy whereas the deletion of either *Psen1* in SMCs or *Psen2* globally attenuates Notch pathway and SMC proliferation, mitigating aortic disease. With SMC-specific *Psen1* deletion in elastin nulls, these rescue effects are more robust and in fact, survival is increased. SMC deletion of *Psen1* also attenuates hypermuscularization in newborns heterozygous for the elastin null gene, which genetically mimics SVAS. Similarly, the pharmacological inhibition of PSEN-1 mitigates SMC accumulation in elastin aortopathy. These findings put forth SMC PSEN-1 as a potential therapeutic target in SVAS.

INTRODUCTION

Defective elastic lamellae and smooth muscle cell (SMC) accumulation are characteristics of diverse arterial diseases, including atherosclerosis, pulmonary hypertension (PH) and supravalvular aortic stenosis (SVAS).[1–5] Although elastin deficiency has been shown to induce SMC hyperproliferation,[2,6] mechanistic links between defective elastic lamellae and SMC hyperproliferation are not well elucidated. Elastin is the major component of circumferential elastic lamellae that alternate with rings of SMCs to form lamellar units in arteries. Heterozygous loss-of-function mutations in elastin gene *ELN* cause SVAS.[7,8] SVAS occurs as an isolated entity or more commonly in Williams-Beuren Syndrome (WBS), which results from a continuous deletion of 26–28 genes on chromosome 7, including *ELN*.[9,10] Elastin mutant mice have been used to model human SVAS.[6] *Eln(−/−)* mice exhibit severe aortic phenotypes with increased medial cellularity and lumen obstruction, resulting in early postnatal death.[6] In contrast, *Eln(+/−)* mice have modest aortic phenotypes with thinner elastic lamellae and additional SMC layers.[11,12] The only treatment for SVAS is major surgery which carries substantial risk of morbidity and mortality,[13] but no pharmacological options are available largely because underlying pathological processes are poorly defined.

The Notch pathway plays integral roles in vascular development and pathology.[14–16] Mammals express four Notch receptors, and NOTCH3 is predominantly expressed in arterial SMCs.[14,17] We recently reported that elastin deficiency upregulates the cleaved form of NOTCH3, resulting in aortic hypermuscularization and stenosis.[18] Cleavage of Notch receptors is catalyzed by gamma-secretase, which is composed of a catalytic presenilin subunit (PSEN-1 or -2) and accessory subunits.[19] Our previous study also demonstrated that the systemic pharmacological inhibition of gamma-secretase attenuates elastin aortopathy.[18] This finding suggests that gamma-secretase inhibition may be a viable therapeutic strategy for SVAS. However, the gamma-secretase inhibitor used in the prior study is likely to attenuate Notch signaling globally and may have off-target effects. Thus, it is desirable to elucidate the individual roles of PSEN-1 and -2 in elastin aortopathy and gain insights into vascular cell type-specific effects.

PSEN-1 and -2 have been extensively studied in Alzheimer's disease because mutations in these genes account for ~90% of the identified mutations in the familial disease.[20] Loss of function of *PSEN1* or *PSEN2* causes incomplete digestion of the amyloid β-peptide, which aggregates into neurotoxic amyloid plaques in the brain.[21] Conditional *Psen1* deletion in the postnatal forebrain of mice leads to memory impairment,[22] whereas global *Psen2* deletion does not have a severe phenotype.[23] Mice with compound deletion of forebrain-specific *Psen1* and global *Psen2* exhibit complete loss of PSEN function in excitatory neurons of the postnatal forebrain and gene dosage-dependent cerebral cortex degeneration.[24,25]

Compared to these brain studies, little is known about the role of PSEN-1 and -2 in the cardiovascular system.[26] *Psen1(−/−)* mice die shortly after birth with intracranial hemorrhage and bone abnormalities,[27] while *Psen2(−/−)* mice are viable and develop mild pulmonary fibrosis.[23] Global *Psen1* deletion causes ventricular septal defect, double outlet right ventricle, and pulmonary artery stenosis at embryonic

[1]Yale Cardiovascular Research Center, Section of Cardiovascular Medicine, Department of Internal Medicine, Yale University, New Haven, CT 06511, USA
[2]Department of Genetics, Yale University, New Haven, CT 06511, USA
[3]Stem Cell Center, Yale University, New Haven, CT 06511, USA
[4]Lead contact
*Correspondence: daniel.greif@yale.edu
https://doi.org/10.1016/j.isci.2023.108636

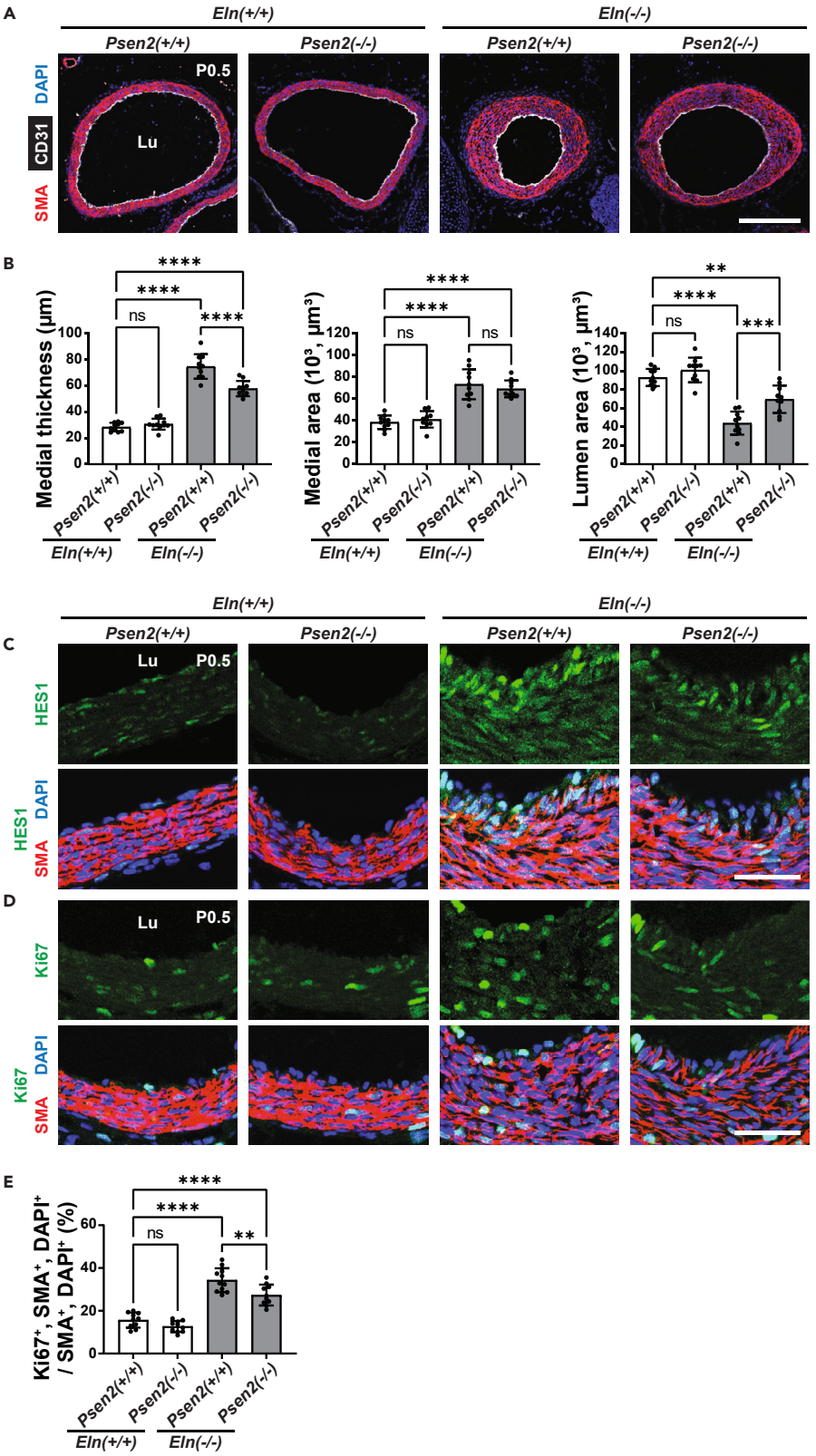
A
Eln(+/+)
Eln(-/-)
Psen2(+/+)
Psen2(-/-)
DAPI
CD31
SMA
P0.5
Lu
B
Medial thickness (μm)
Medial area (10³, μm³)
Lumen area (10³, μm³)
ns
****
**
***
Psen2(+/+)
Psen2(-/-)
Eln(+/+)
Eln(-/-)
C
HES1
SMA
DAPI
D
Ki67
E
Ki67⁺, SMA⁺, DAPI⁺ / SMA⁺, DAPI⁺ (%)

Figure 1. In *Eln* null, *Psen2* deletion attenuates aortic hypermuscularization, stenosis and SMC proliferation

Transverse sections of the ascending aorta (cranial position, Figure S2) from pups at P0.5 of indicated genotype were analyzed.

(A) Sections were stained for SMA, CD31 (EC marker), and nuclei (DAPI).

(B) Histograms represent aortic medial wall thickness, medial area and lumen area from sections as shown in A. n = 10 mice.

(C and D) Sections were stained for SMA, nuclei (DAPI), and either HES1 in C or Ki67 (marker of proliferation) in D.

(E) Histograms represent percent of SMCs that are $Ki67^{+}$ from sections represented by D. n = 10–13 mice. Lu, lumen. ns, not significant. **p < 0.01, ***p < 0.001, ****p < 0.0001 by multifactor ANOVA with Tukey's *post hoc* test. Data are presented as mean ± SD. Scale bars, 200 μm (A) and 40 μm (C, D).

day (E) 12.5–15.5,[28] whereas global knockout of both *Psen1* and *Psen2* induces an un-looped heart at E8.5–9.0.[29] In contrast, combined *Psen1* deletion in adult mice with inducible $CreER^{T2}$, which is expressed under the RNA polymerase II promoter, and global *Psen2* deletion protects against angiotensin II-induced cardiac hypertrophy.[30] Thus, PSEN1 and PSEN2 play key roles in embryogenesis of the heart and vasculature and pathogenesis of adult cardiovascular disease. However, vascular cell type-specific *Psen1* deletion in any context and the specific roles of PSEN1 and PSEN2 in elastin aortopathy have not been elucidated.

Our current study reports that PSEN-1 and -2 are upregulated in aortic SMCs with elastin insufficiency in human and mouse. Using mouse models, we demonstrate that global *Psen2* deletion partially attenuates aortic hypermuscularization and stenosis in *Eln(−/−)* mutants and *Psen1* deletion in SMCs more significantly mitigates this aortopathy and improves survival. In contrast, *Psen1* deletion in endothelial cells (ECs) does not improve elastin aortopathy. The combination of global *Psen2* deletion and SMC-specific *Psen1* deletion has additive rescue effects on hypermuscularization and stenosis in the elastin-deficient aorta. SMC-specific *Psen1* deletion also rescues hypermuscularization in *Eln(+/−)* mutants. Similarly, the pharmacological inhibition of PSEN-1 mitigates SMC accumulation in the elastin mutant aorta. These findings suggest that SMC PSEN-1 plays a main role in elastin aortopathy, providing pre-clinical insight that may facilitate therapeutic strategies to improve efficacy and mitigate off-target effects of gamma-secretase inhibition in this context.

RESULTS

Elastin deficiency upregulates presenilin subunits of gamma-secretase

We previously reported that elastin deficiency promotes the cleavage of NOTCH3, resulting in aortic hypermuscularization and stenosis, and that the pharmacological inhibition of gamma-secretase attenuates elastin aortopathy.[18] Herein, we initially assessed the effect of reduced elastin levels on gamma-secretase subunits PSEN-1 and -2 in human aortic SMCs. Human aortic SMCs were treated with scrambled (Scr) RNA or *ELN*-specific silencing RNA (siRNA) and subjected to quantitative real-time reverse transcription PCR (qRT-PCR) and Western blotting. *ELN* silencing increased transcript and protein levels of PSEN-1 and -2 (Figures S1A and S1B). We further analyzed the levels of PSEN-1 and -2 with reduced elastin gene dosage in mice. Aortas were isolated from wild type (WT) or *Eln(−/−)* pups on postnatal day 0.5 (P0.5), and aortic lysates were analyzed by qRT-PCR and Western blotting. Compared to WT, *Eln(−/−)* aortas had higher levels of transcripts (~6-fold) and protein (~1.7-fold) for both PSEN-1 and -2 (Figures S1C and S1D). Transverse sections of ascending aortas from WT and *Eln(−/−)* pups at P0.5 were stained for PSEN-1 or -2, confirming their upregulation with elastin deficiency (Figure S1E). These data demonstrate that insufficient elastin in SMCs results in upregulated PSEN-1 and -2.

Ascending aorta morphology at different cranio-caudal levels in elastin mutants

Similar to SVAS, the hallmark of *Eln(−/−)* newborns is ascending aortic hypermuscularization and stenosis[6,18]; however, a systematic evaluation of the *Eln* null ascending aorta at discrete positions has not been reported. We analyzed serial transverse sections of the ascending aorta from WT or *Eln(−/−)* pups at P0.5 (Figure S2). We report three positions: 1) cranial – immediately below the aortic arch; 2) middle – between cranial and caudal positions; 3) caudal – where the main pulmonary artery crosses the ascending aorta (Figure S2A). Our analysis revealed that *Eln(−/−)* ascending aorta at the cranial position has the most significant phenotype with increased medial thickness and area and decreased lumen area compared to WT (Figures S2B and S2C). Thus, we analyzed the cranial position of the ascending aorta in all following experiments.

Presenilin*2* deletion partially attenuates aortic hypermuscularization and smooth muscle cell proliferation in elastin mutant aortas

To elucidate the role of PSEN-1 and -2 in elastin aortopathy, we analyzed the effect of *Psen* deletion on the *Eln(−/−)* background. Since *Psen1(−/−)* mice die immediately after birth,[27] we started by analyzing *Psen2* global nulls.[23] Note the Greif lab received *Psen1(flox/flox)*, *Psen2(−/−)* mice from the Shen lab, and all studies of *Psen2* mutants were performed on the *Psen1(flox/flox)* background. *Eln(+/−)*, *Psen2(+/−)* mice were bred together, pups were harvested at P0.5, and the transverse cryosections of the ascending aorta (cranial position, see Figure S2) were analyzed. Consistent with our previous study,[18] on the *Psen2(+/+)* background, compared to *Eln(+/+)* aorta, *Eln(−/−)* aorta has 2.5-fold increased medial wall thickness and 60% reduction of lumen area (Figures 1A and 1B). Global *Psen2* deletion does not alter aortic phenotype on the *Eln(+/+)* background, whereas *Eln(−/−)*, *Psen2(−/−)* mutants had a 23 ± 8% reduction in medial thickness and 158 ± 33% increase in lumen area compared to *Eln(−/−)*, *Psen2(+/+)* mice at P0.5 (Figures 1A and 1B).

Immunostains for HES1 (a NOTCH signaling target molecule) demonstrate that elastin deficiency upregulates HES1 expression (Figure 1C). SMCs in the inner part of the medial wall are misaligned in a radial orientation,[31] and interestingly, HES1 was most upregulated in this region (Figure 1C). The expression of HES1 was partially attenuated by *Psen2* deletion (Figure 1C). Since PSEN-2 is completely abolished in *Psen2(−/−)*

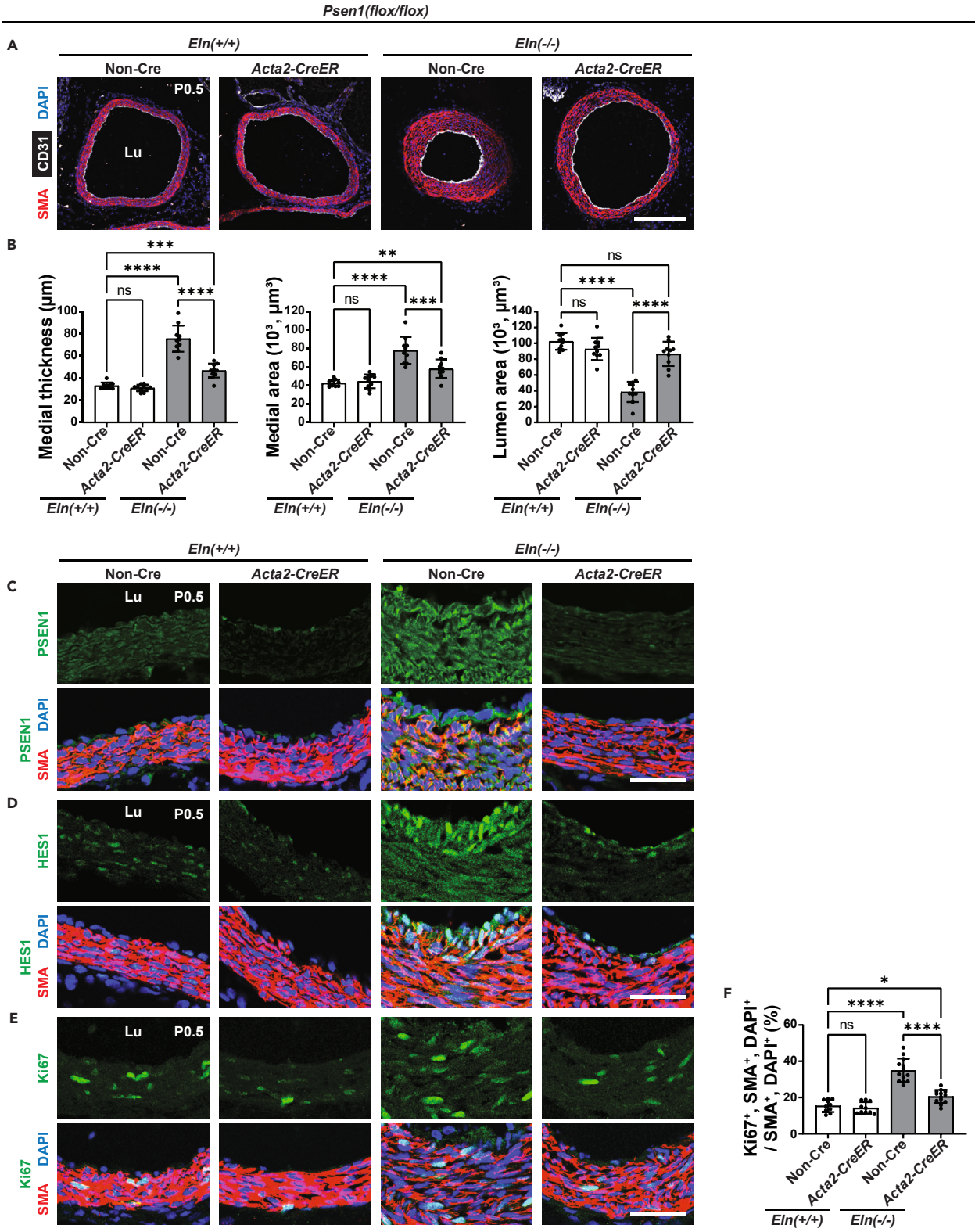

Figure 2. On the *Eln(−/−)* background, SMC-specific *Psen1* deletion reduces hypermuscularization, stenosis and SMC proliferation

Transverse sections of the ascending aorta (cranial position, Figure S2) from pups at P0.5 of indicated genotype were analyzed.

(A) Sections were stained for SMA, CD31, and nuclei (DAPI).

Figure 2. *Continued*

(B) Histograms represent aortic medial wall thickness, medial area and lumen area from sections as in A. n = 10 mice.

(C–E) Sections were stained for SMA, nuclei (DAPI), and either PSEN1 in C, HES1 in D, or proliferation marker Ki67 in E.

(F) Histograms represent percent of SMCs that are Ki67$^+$ from sections represented by E. n = 10–13 mice. Lu, lumen. ns, not significant. *p < 0.05, **p < 0.01, ***p < 0.001, ****p < 0.0001 by multifactor ANOVA with Tukey's *post hoc* test. Data are presented as mean ± SD. Scale bars, 200 μm (A) and 40 μm (C-E).

aorta (Figure S3), the remaining expression of HES1 likely reflects PSEN-1 activity. Immunostaining for the proliferation marker Ki67 indicates that *Psen2* deletion modestly reduces elastin deficiency-induced SMC proliferation (Figures 1D and 1E). Taken together, *Psen2* global deletion partially attenuates elastin aortopathy.

Presenilin*1* deletion with *Acta2-CreER^{T2}*, but not *Cdh5-CreER^{T2}*, attenuates elastin aortopathy

As global *Psen2* deletion partially rescues elastin aortopathy (Figure 1) and *Psen1* null mice die immediately after birth,[27] we next evaluated the effect of *Psen1* deletion specifically in ECs or SMCs. For the investigation of EC PSEN-1, *Psen1(flox/flox)* pups that were also carrying no Cre or inducible *Cdh5-CreER^{T2}* and either *Eln(+/+)* or *Eln(−/−)* were analyzed (Figure S4). We injected pregnant dams at embryonic day (E) 14.5 and E15.5 with 1 mg of tamoxifen and concomitant 0.25 mg of progesterone to minimize the incidence of dystocia.[18,31] At P0.5, newborns were genotyped, and the ascending aortas were sectioned transversely and stained for SMA and CD31. The *Eln(−/−)* aortic phenotype was not altered by the EC deletion of *Psen1* (Figures S5A and S5B). Immunostaining revealed that *Psen1* deletion in ECs changes neither PSEN1 expression nor Ki67$^+$ SMCs in the media (Figures S5C–S5F). Thus, EC PSEN1 is not requisite for elastin aortopathy.

To determine the role of PSEN1 in SMCs on elastin aortopathy, *Psen1(flox/flox)* pups that were also carrying no Cre or the inducible *Acta2-CreER^{T2}* and either *Eln(+/+)* or *Eln(−/−)* were generated (Figure 2). Injections of tamoxifen and progesterone at E14.5 and E15.5 [18,31] led to a robust reduction of PSEN1 in aortic SMCs at P0.5 (Figure S6). At this time point, the ascending aortas were sectioned transversely and stained for SMA and CD31. In comparison with *Psen1(flox/flox), Eln(+/+)* controls, the medial thickness and area of *Psen1(flox/flox), Eln(−/−)* newborns were increased and the lumen area was decreased. These changes were markedly attenuated in *Acta2-CreER^{T2}, Psen1(flox/flox), Eln(−/−)* pups (Figures 2A and 2B). Quantitative analysis revealed that on the *Psen1(flox/flox), Eln(−/−)* background, the presence of *Acta2-CreER* leads to a 38 ± 8% reduction in medial thickness, 26 ± 13% reduction in medial area and 225 ± 40% increase in lumen area (Figure 2B). Notably, in *Eln(+/+)* mice, SMC *Psen1* deletion does not influence aortic morphology. Deletion of *Psen1* in SMCs of elastin nulls leads to decreased medial HES1 expression and Ki67$^+$ SMCs (Figures 2C–2F). These findings suggest that SMC *Psen1* is integral to the pathogenesis of elastin aortopathy.

Presenilin*1* deletion with *Acta2-CreER^{T2}* further attenuates aortic hypermuscularization and stenosis in presenilin*2(−/−), Eln(−/−)* mice

As a murine pathological model of Alzheimer's disease, the genetic deletion of *Psen1* in the forebrain leads to a compensatory upregulation of *Psen2*, and compound global *Psen2* deletion is required to induce cortical volume reduction.[24] Thus, we assessed the combined effect of global *Psen2* deletion and vascular cell type-specific *Psen1* deletion in elastin aortopathy. For EC-specific *Psen1* deletion, *Psen1(flox/flox), Psen2(−/−)* pups that were also carrying no Cre or inducible *Cdh5-CreER^{T2}* and either *Eln(+/+)* or *Eln(−/−)* were analyzed (Figure S7). Pregnant dams were injected at E14.5 and E15.5 with tamoxifen and progesterone as described above,[18,31] and pups were analyzed at P0.5. The aortic phenotype of *Psen1(flox/flox), Psen2(−/−), Eln(−/−)* pups is not altered by the presence of *Cdh5-CreER^{T2}* (Figures S7A and S7B). Immunostaining also revealed that the expression of PSEN-1, HES1 and Ki67 in the media is not changed by EC-specific *Psen1* deletion (Figures S7C–S7F), suggesting that EC PSEN-1 does not have additional rescue effects in *Psen2(−/−), Eln(−/−)* pups.

To determine the role of PSEN-1 in SMCs on *Eln(−/−), Psen2(−/−)* background, a similar experiment was conducted with *Acta2-CreER^{T2}* substituting for *Cdh5-CreER^{T2}* (Figure 3). In comparison with *Psen1(flox/flox), Psen2(−/−), Eln(−/−)* newborns, *Acta2-CreER^{T2}, Psen1(flox/flox), Psen2(−/−), Eln(−/−)* pups have attenuated medial thickness and area and increased lumen area (Figures 3A and 3B). Immunostaining demonstrated marked reduction in the expression of PSEN-1 and HES1 and quantity of Ki67$^+$ SMCs in the media (Figure S8). These findings indicate additional rescue effects of SMC-specific *Psen1* deletion on *Psen2(−/−), Eln(−/−)* background.

To directly compare effects of global *Psen2* deletion, SMC-specific *Psen1* deletion and the combination, we combined data of Figures 1B, 2B, and 3B in Figure S9. On the elastin null background, SMC-specific *Psen1* deletion is more effective than global *Psen2* deletion in terms of preventing medial thickness and preserving lumen area (Figure S9). The combination of global *Psen2* and SMC-specific *Psen1* deletion shows the most effective rescue of medial thickness compared with each individual gene deletion (Figure S9). Quantitative analysis revealed that compound *Acta2-CreER^{T2}, Psen1(flox/flox), Psen2(−/−), Eln(−/−)* mutants have a 49 ± 7% reduction in medial thickness, 32 ± 9% reduction in medial wall area and 229 ± 28% increase in lumen area in comparison with *Psen1(flox/flox), Psen2(+/+), Eln(−/−)* mice (Figure S9).

Immunostains demonstrate that elastin deficiency upregulates HES1 expression in the inner part of the medial wall (Figures 1C, 2D, S5D, S7D, and S8B). Consistent with this finding, another NOTCH target molecule HEY1 as well as the intracellular domain of NOTCH3 (NICD3; active form of NOTCH3) are upregulated in this region in *Eln* null mice (Figure S10). Note that NICD3 is demonstrated by the overlap of staining for NOTCH3 and nuclei (DAPI).[32] HEY1 and NICD3 are attenuated by the compound deletion of *Psen2* globally and *Psen1* in SMCs (Figure S10). Although *Psen* deletion efficiently attenuates NOTCH signaling (Figure S10) and improves ascending aortic phenotype in *Eln(−/−)* pups (Figure S9), immunostaining for other extracellular components, such as collagens I, IV, VI and VIII, is not altered (Figure S11).

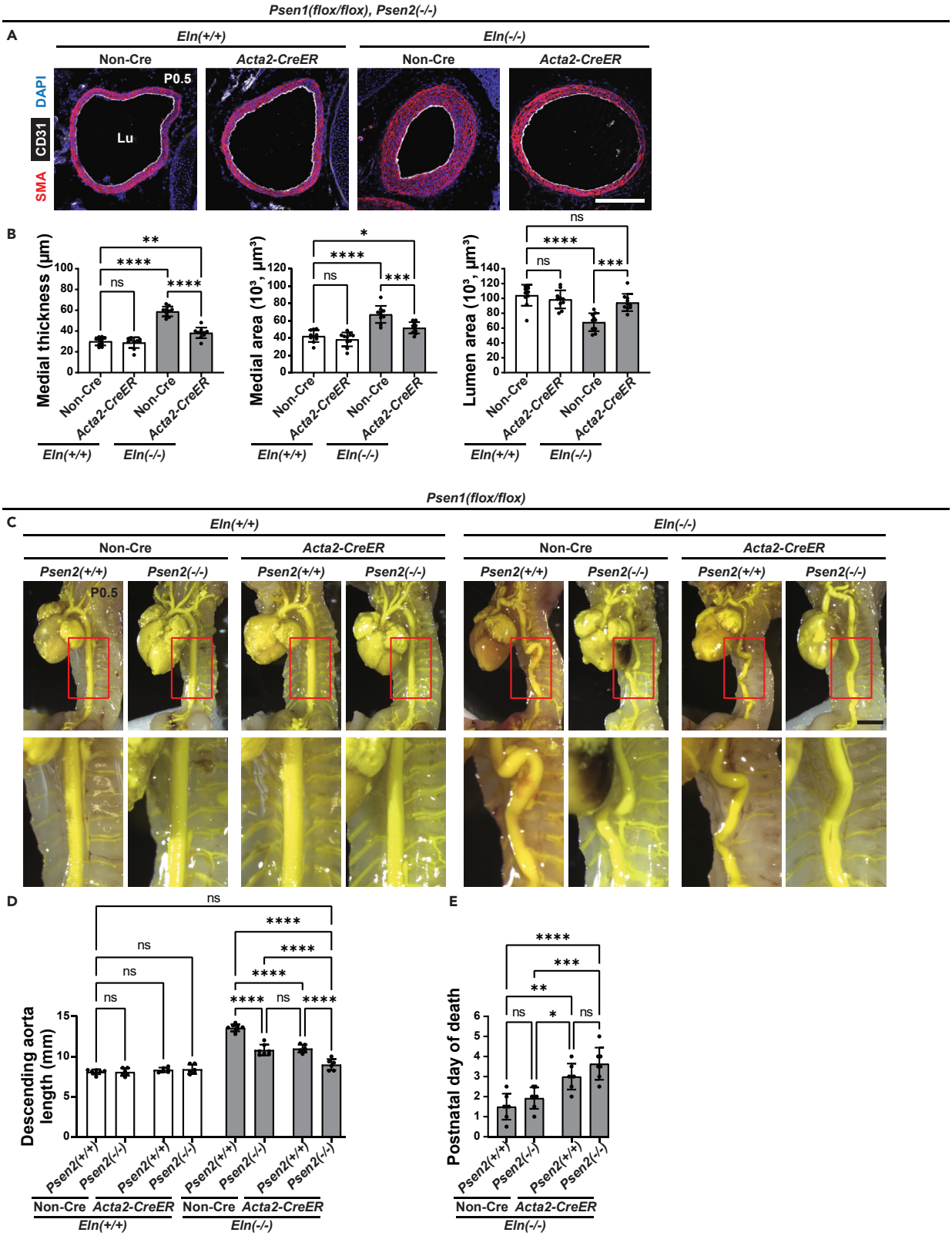
Psen1(flox/flox), Psen2(-/-)
A
Eln(+/+)
Eln(-/-)
Non-Cre
Acta2-CreER
Non-Cre
Acta2-CreER
P0.5
DAPI
CD31
SMA
Lu
B
Medial thickness (μm)
Medial area (10³, μm³)
Lumen area (10³, μm³)
ns
**
****
***
*
Non-Cre
Acta2-CreER
Eln(+/+)
Eln(-/-)
Psen1(flox/flox)
C
Eln(+/+)
Eln(-/-)
Non-Cre
Acta2-CreER
Psen2(+/+)
Psen2(-/-)
P0.5
D
Descending aorta length (mm)
E
Postnatal day of death

Figure 3. On the *Eln(−/−), Psen2(−/−)* background, SMC-specific *Psen1* deletion further attenuates aortopathy and extends viability

(A) Transverse sections of the ascending aorta (cranial position, Figure S2) from pups at P0.5 of indicated genotype were stained for SMA, CD31 and nuclei (DAPI). Lu, lumen.

(B) Histograms represent aortic medial wall thickness, medial area and lumen area from sections as in A. n = 10 mice.

(C) Gross descending aorta morphology was visualized by injecting yellow latex into the left ventricle of newborns of indicated genotypes at P0.5. Lower images are the magnifications of the red boxes.

(D) Histograms represent the length of the descending aorta from the left brachiocephalic artery to the celiac artery in pups with indicated genotypes at P0.5. n = 6–8 mice.

(E) The age of death of newborns with indicated genotypes is depicted. n = 7 mice. ns, not significant. *p < 0.05, **p < 0.01, ***p < 0.001, ****p < 0.0001 by multifactor ANOVA with Tukey's *post hoc* test. Data are presented as mean ± SD. Scale bars, 200 μm (A) and 2 mm (C).

Compound presenilin deletion attenuates aortic tortuosity and extends the viability of *Eln(−/−)* mice

Thus far, our findings suggest that the combination of SMC *Psen1* and global *Psen2* deletion significantly attenuates the ascending aortic phenotype of *Eln(−/−)* mice. In addition to ascending aorta stenosis, tortuosity of the descending aorta is another hallmark in *Eln(−/−)* mice.[33] This tortuosity results from less axial stress and increased SMC proliferation.[34] To visualize the descending aorta morphology, yellow latex was injected through the left ventricle at P0.5.[35] Consistent with previous literature,[33] *Eln(−/−)* mice have a severely tortuous descending aorta compared to *Eln(−/−)* mice (Figure 3C) without altering body weight or length (Figure S12). In elastin WT, neither SMC *Psen1* deletion nor global *Psen2* deletion influences descending aorta tortuosity (Figures 3C and 3D). On *Eln(−/−)* background, SMC *Psen1* deletion or global *Psen2* deletion attenuates the tortuosity, and importantly, the combination of these deletions is additive (Figures 3C and 3D).

Even though either SMC *Psen1* deletion or compound deletion of SMC *Psen1* and global *Psen2* markedly rescues *Eln(−/−)* aortic phenotypes, extension of survival is modest (Figure 3E). In addition to the aortic phenotypes, severe emphysema is observed in *Eln(−/−)* pups.[36,37] This lung phenotype is not rescued by compound *Psen* deletion (Figures S13A and S13B) and thus, may explain the limited extension of survival in *Eln* nulls (Figure 3E).

Compound smooth muscle cell presenilin*1* and global presenilin*2* deletion attenuates hypermuscularization in *Eln(+/−)* ascending aorta

In contrast to *Eln(−/−)* mice, *Eln(+/−)* mice display normal lung development.[38] Importantly, human SVAS is caused by heterozygous elastin gene mutations and lacks parenchymal lung disease.[7,9,11] Thus, we assessed the effect of genetic *Psen* deletion in *Eln(+/−)* mice. Although *Eln(+/−)* murine aorta does not have as significant a phenotype as human SVAS, mild hypermuscularization and stenosis are observed in these mice compared to WT mice (Figure 4). In *Eln(+/−)* mice, SMC *Psen1* deletion, but not global *Psen2* deletion, attenuates hypermuscularization (Figure 4).

Pharmacological inhibition of presenilin-1 mitigates aortic smooth muscle cell accumulation in elastin mutants

Given the important role of PSEN-1 in elastin aortopathy, we next evaluated the effect of the PSEN inhibitor MRK-560, which has ~100-fold selectivity for PSEN-1 over PSEN-2,[39] in this context. MRK-560 was initially injected intraperitoneally in pregnant dams on E14.5 and E15.5, resulting in intracranial hemorrhage in all pups at P0.5 (Figures S14A–S14C). This phenotype may reflect the brain phenotype (i.e., intracranial hemorrhage) of *Psen1(−/−)* mice.[27] Thus, we instead injected MRK-560 at E16.5 and E17.5, which does not induce an observable brain phenotype in neonates (Figures S14D–S14F). Pups were collected at P0.5, and the ascending aortas were sectioned transversely and stained for SMA and CD31. On the *Eln(+/+)* background, MRK-560 does not influence ascending aorta morphology (Figures 5A and 5B). In contrast, MRK-560 attenuates medial wall thickness and medial area in *Eln(+/−)* and *Eln(−/−)* mice and increases aortic lumen area in *Eln* nulls (Figures 5A and 5B). Immunostains show marked reduction in HES1 expression (Figure 5C) and the quantity of $Ki67^+$ SMCs in the media (Figures 5D and 5E) with the pharmacological PSEN-1 inhibition of *Eln(−/−)* mice. Echocardiography revealed increased ascending aorta peak velocity and decreased cardiac stroke volume in *Eln(−/−)* pups at P0.5, and these hemodynamic parameters were improved by MRK-560 treatment (Figure S15A). Although MRK-560 markedly improves ascending aorta morphology and hemodynamics in *Eln(−/−)* pups, it does not mitigate lung emphysema (Figures S15B and S15C), similar to genetic *Psen* deletion (Figures S13A and S13B).

Finally, we evaluated whether MRK-560 reverses established aortic muscularization in *Eln(+/−)* neonates. As shown in Figure 4, *Eln(+/−)* pups exhibit a mildly hypermuscularized aorta compared to *Eln(+/+)* littermates at P0.5. *Eln(+/+)* or *Eln(+/−)* pups were injected daily with MRK-560 or vehicle from P2.5–6.5, and were collected at P8.5 (Figure 6A). MRK-560 markedly reduces aortic medial wall thickness and SMC proliferation in *Eln(+/−)*, but not in *Eln(+/+)*, mice (Figures 6B–6D). Brain structure (as evaluated by H&E staining) and body weight are not altered by MRK-560 (Figures 6E and 6F). Taken together, pharmacological PSEN-1 selective inhibition has a therapeutic potential for elastin aortopathy.

DISCUSSION

We recently reported that elastin deficiency leads to decreased DNA methylation on promoters of *PSEN-1* and *-2* and increased protein levels of these subunits in human aortic SMCs.[18] The current study demonstrates that reduced elastin dosage upregulates mRNA and protein levels of both PSEN-1 and -2 in human and mouse aortic SMCs (Figure S1) and that the elastin mutant aortic phenotype is rescued substantially by the deletion of SMC *Psen1* and partly by the global deletion of *Psen2* (Figures 1, 2, 3, and 4). Aortic SMC accumulation is also attenuated by the pharmacological inhibition of PSEN-1 (Figures 5 and 6). Thus, SMC PSEN-1 plays a major role in the pathogenesis of elastin aortopathy.

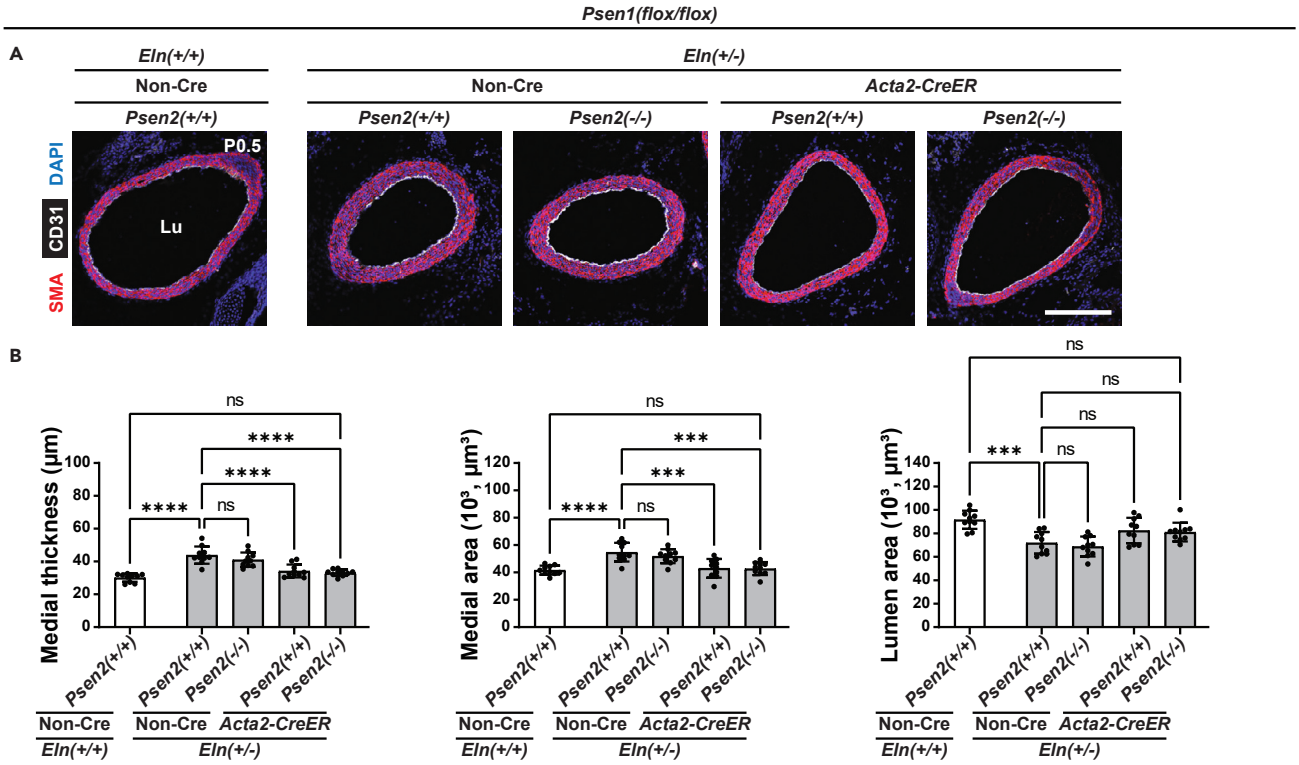

Figure 4. Deletion of *Psen1* in SMCs mitigates hypermuscularization in *Eln(+/−)* mice

(A) Transverse sections of the ascending aorta (cranial position, Figure S2) from pups of indicated genotype at P0.5 were stained for SMA, CD31 and nuclei (DAPI). Lu, lumen. Scale bar, 200 μm.

(B) Histograms represent aortic medial wall thickness, medial area and lumen area from sections represented by A. n = 10 mice. ns, not significant. ***p < 0.001, ****p < 0.0001 by multifactor ANOVA with Tukey's *post hoc* test. Data are presented as mean ± SD.

PSEN-1 and -2 are expressed ubiquitously at comparable levels in most human and mouse tissues.[40] They have similar structure, sharing 63% of amino acid residues at identical positions[41,42]; however, PSEN-1 is essential, whereas PSEN-2 is redundant, during development. This difference may derive from distinct subcellular localization patterns of the PSENs. PSEN-1 is present at the plasma and endosomal membranes, whereas PSEN-2 is mainly restricted to the endosomal membrane via an ERTSML motif in the N-terminus.[43] Indeed, the higher expression of PSEN1 at the plasma membrane, where Notch receptors are located, may explain why Notch receptor cleavage has been shown to be more dependent on PSEN-1 than PSEN-2 in blastocyst cultures.[44] *Psen1(−/−)* pups die at P0.5 with brain hemorrhage and bone abnormalities,[27] whereas *Psen2* nulls develop mild pulmonary fibrosis during adulthood.[23] The phenotype of *Psen1(−/−)* mice is worsened by *Psen2* deletion as compound *Psen1* and *Psen2* nulls have severe growth retardation at E9.5 and die soon thereafter.[23] Our study indicates that ~70% reduction of PSEN-1 in SMCs markedly improves elastin aortopathy (Figures 2 and S6), while global *Psen2* nulls have mild effects (Figure 1).

From a clinical perspective, our current and previous studies[18] suggest that gamma-secretase inhibition is a potential therapeutic strategy for SVAS/WBS. Pre-clinical studies of gamma-secretase inhibitors have shown some benefit in cancer[45]; however, there are dose-dependent toxicities, including severe diarrhea,[46,47] skin infections,[48] and lymphocyte abnormalities.[49–51] These adverse effects are due to the systemic inhibition of gamma-secretase. As an enzymatic subtype, each gamma-secretase molecule contains one catalytic subunit, PSEN-1 or PSEN-2.[52] The predominant gamma-secretase subtype in human T cell acute lymphoblastic leukemia (T-ALL) contains PSEN-1.[53] In a mouse model of T-ALL, a recently developed PSEN-1 selective inhibitor MRK-560 significantly attenuates disease progression and extends survival and in comparison to a broad-spectrum gamma-secretase inhibitor, reduces adverse effects.[53] In the context of elastin aortopathy, SMC PSEN-1 is a major contributor to hypermuscularization, more so than PSEN-2 (Figure S9). It is also important that SMC-specific *Psen1* deletion reduces hypermuscularization in *Eln(+/−)* mice, whereas global *Psen2* deletion does not (Figure 4). Similarly, *Eln(+/−)* aortic hypermuscularization is markedly attenuated by MRK-560 (Figures 5 and 6). As human SVAS is caused by heterozygous loss-of-function *ELN* mutations,[7] these findings suggest that PSEN-1 selective inhibition may be a promising therapeutic strategy, with reduced adverse effects compared to broad gamma-secretase inhibition.

Gamma-secretase exhibits relatively poor substrate specificity, and in fact, this enzyme cleaves ~150 different molecules.[54] In contrast to Notch receptors, most of these substrates have been primarily evaluated in cell lines (e.g., HEK293 and MEF),[54] and their potential functions in the vasculature are not elucidated. Gamma-secretase cleaves vascular endothelial growth factor receptor (VEGFR)-1 in bovine retinal microvascular ECs and is suggested to negatively regulate VEGFR-2-driven neovascularization.[55,56] Other angiogenesis-related molecules (e.g., erb-b2

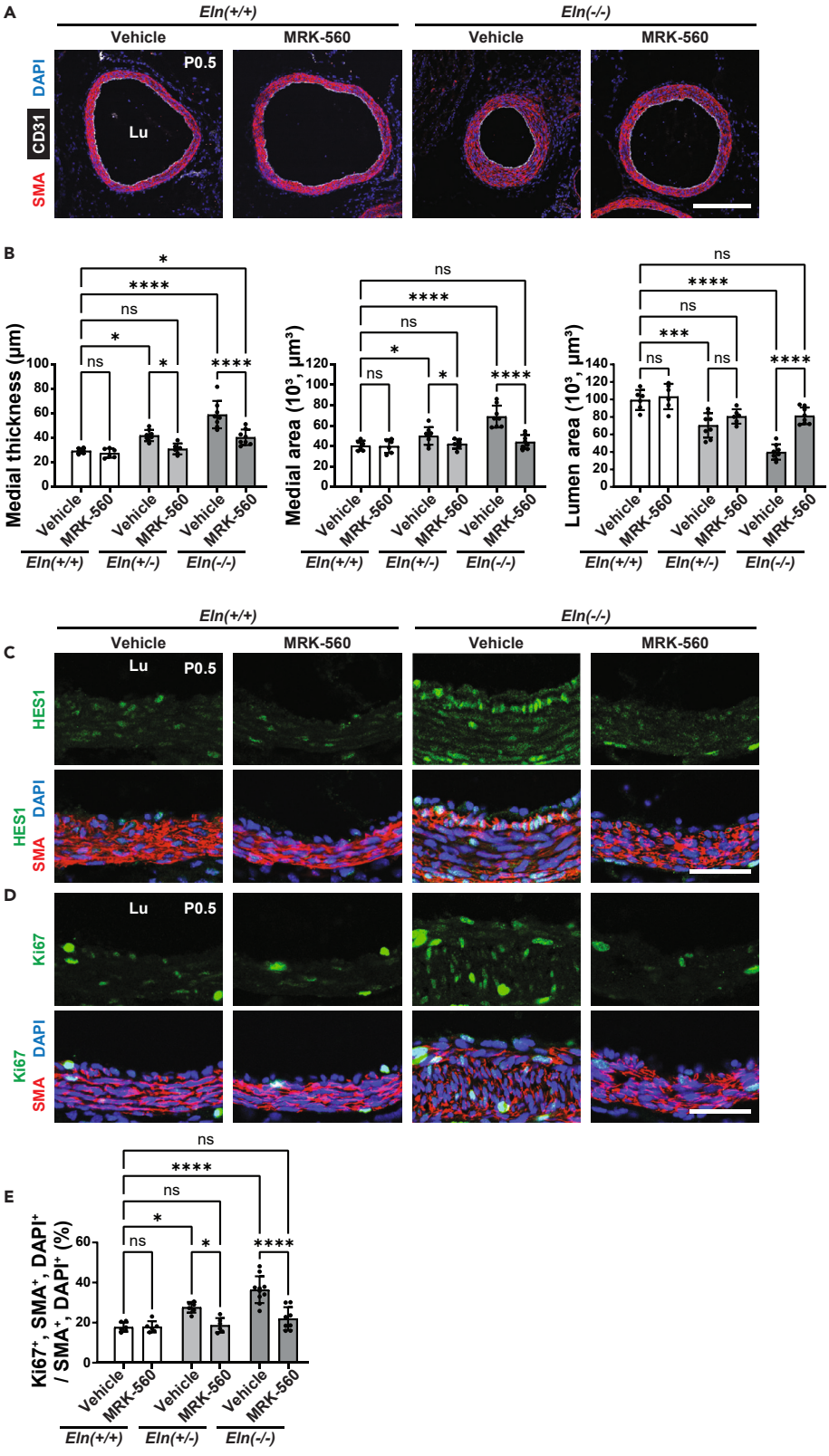
A
Eln(+/+)
Eln(-/-)
Vehicle
MRK-560
Vehicle
MRK-560
DAPI
CD31
SMA
P0.5
Lu
B
Medial thickness (μm)
Medial area (10³, μm³)
Lumen area (10³, μm³)
ns
*
****
***
Vehicle
MRK-560
Eln(+/+)
Eln(+/-)
Eln(-/-)
C
HES1
DAPI
SMA
D
Ki67
E
Ki67⁺, SMA⁺, DAPI⁺ / SMA⁺, DAPI⁺ (%)

Figure 5. MRK-560 treatment on E16.5 and E17.5 reduces hypermuscularization, stenosis and SMC proliferation in elastin mutant neonates

Pregnant dams bearing *Eln(+/+)*, *Eln(+/−)* or *Eln(−/−)* embryos were injected on E16.5 and E17.5 with either vehicle or PSEN-1 selective inhibitor MRK-560, and pups were collected at P0.5. Transverse sections of the ascending aorta (cranial position, Figure S2) from pups at P0.5 of indicated genotype and/or treatment were analyzed. (A) Sections were stained for SMA, CD31, and nuclei (DAPI).

(B) Histograms represent aortic medial wall thickness, medial area and lumen area from sections as in A. n = 6–8 mice.

(C and D) Sections were stained for SMA, nuclei (DAPI), and either HES1 in C or proliferation marker Ki67 in D.

(E) Histograms represent percent of SMCs that are $Ki67^+$ from sections represented by D. n = 6–10 mice. Lu, lumen. ns, not significant. *p < 0.05, ***p < 0.001, ****p < 0.0001 by multifactor ANOVA with Tukey's *post hoc* test. Data are presented as mean ± SD. Scale bars, 200 μm (A) and 40 μm (C, D).

receptor tyrosine kinase 4 and insulin-like growth factor-1 receptor) are also cleaved by gamma-secretase; however, these cleavages were observed in non-vascular cell types, and physiological functions of these proteolytic events are not yet determined.[57,58] Intracellular domains of some gamma-secretase substrates (e.g., Notch receptors) can enter the nucleus and modulate gene expression and cell growth.[54] The potential effects of cleavage of diverse substrates will need to be considered in moving the strategy of PSEN-1 inhibition forward in clinical applications.

Reduced gene dosage of SMC *Psen1* alone or of SMC *Psen1* and global *Psen2* in combination extends the survival of *Eln(−/−)* mice (Figure 3), which is likely attributable to improved hemodynamics. Our data reveal that the deletion of *Psen1/2* ameliorates ascending aorta stenosis as well as descending aorta tortuosity (Figures 1, 2, and 3). No prior studies have demonstrated rescue of elastin deficiency-induced descending aorta tortuosity. Similar to ascending aorta hypermuscularization and resultant stenosis, descending aorta tortuosity is associated with excess SMC proliferation[34] and indeed, may be another useful parameter for evaluating genetic/pharmacological interventions in elastin aortopathy. Consistent with ascending aortic stenosis, echocardiography indicates increased ascending aorta peak velocity and reduced stroke volume in *Eln(−/−)* mice at P0.5, and MRK-560 treatment improves these hemodynamics (Figure S15A). In *Eln* nulls, the extension of survival with *Psen* deletion is limited to ~2 days. In addition to the aortic phenotype, *Eln(−/−)* pups also exhibit severe emphysema,[36,37] and compound deletion of SMC-*Psen1* and global *Psen2* is insufficient to overcome this lung phenotype (Figure S13). In contrast to *Eln(−/−)* mice, human SVAS/WBS, which is caused by *ELN* haploinsufficiency, is not associated with parenchymal lung disease.[7,9,11] Similar to patients with SVAS/WBS, *Eln(+/−)* mice display normal lung development,[38] and importantly, deletion of SMC-*Psen1* or pharmacological PSEN-1 inhibition reduces *Eln(+/−)* aortic phenotypes (Figures 4, 5, and 6).

The Notch downstream molecules HES1 and HEY1 as well as NICD3 are markedly enhanced in the inner media of *Eln(−/−)* aorta (e.g., Figures 1C, 2D, 5C, S5D, S7D, and S10), where SMCs exhibit radial orientation.[31] We previously reported that integrin β3 is similarly enhanced in these SMCs.[31] Our working model is that NICD3 binds to *Itgb3* promoter and increases expression,[18,31] and thus, the activity of gamma-secretase may be anticipated to be enhanced in the inner media of the *Eln(−/−)* aorta. However, our data demonstrate that PSEN-1 and -2 are upregulated throughout *Eln(−/−)* aortic media, and thus, localized upregulation of Notch signaling and integrin β3 is not explained by the PSEN-1 and -2 distribution. Although a clear explanation is not yet evident, we speculate on a number of possibilities for this localization. The first possibility for localized Notch activation and integrin β3 in the inner media is the proximity to ECs. EC-secreted factors, including platelet-derived growth factor-B, transforming growth factor β, and sphingosine-1-phosphate, promote SMC recruitment during embryogenesis.[59] Among these factors, shingosine-1-phosphate has been shown to activate the Notch pathway, upregulating HES1 in cancer stem cells.[60] In addition, contact between ECs and SMCs leads to SMC differentiation through Notch receptors[61] and connexins.[62,63] Importantly, our previous study demonstrated that the Notch ligand JAG1 is significantly upregulated in ECs of the elastin null aorta, which may activate Notch receptors in SMCs of the inner aortic media.[18] Another possible explanation for localized Notch activation in the inner layers is the heterogeneous SMC populations in the ascending aortic media. Lineage-tracing experiments of *Eln(+/+)* mice demonstrate that the second heart field (SHF)-derived cells populate the outer media of the ascending aorta, while cardiac neural crest (CNC)-derived cells populate the inner media of the anterior region and contribute transmurally to the media posteriorly.[64] A recent study of *Eln* deletion in SHF- or CNC-derived SMCs suggest that SHF-derived SMCs significantly contribute to neointima in the ascending aorta, while CNC-derived SMCs induce medial wall thickening and sporadic neointima.[35] This study also performed single cell RNA-seq of *Tagln-Cre, Eln(flox/flox)* ascending aorta and identified SMC subpopulations in the neointima.[35] We speculate that select SMC subpopulations with elastin deficiency may potentially promote the activity of gamma-secretase, resulting in the localized upregulation of Notch signaling and integrin β3.

The finding that PSEN-1 in SMCs plays a major role in hypermuscularization in elastin aortopathy may provide insights into the therapeutic strategies for other proliferative vascular diseases, such as pulmonary hypertension (PH). Interestingly, NOTCH3 expression is upregulated in pulmonary arterial SMCs in human and murine PH.[65] Furthermore, gamma-secretase inhibition significantly reduces hypoxia-induced PH in mice by attenuating the activation of NOTCH3 in SMCs.[65] Although the specific catalytic subunit of gamma-secretase involved in PH has not been elucidated, our study suggests that SMC PSEN-1 may play a key role.

In summary, elastin insufficiency in SMCs leads to the upregulation of PSEN-1 and -2, which induce Notch signaling and SMC proliferation. Deletion of SMC *Psen1* robustly rescues and global deletion of *Psen2* partly ameliorates aortic hypermuscularization and stenosis of *Eln(−/−)* mice. Similarly, pharmacological PSEN-1 inhibition ameliorates aortic SMC accumulation in elastin mutant mice. Thus, inhibiting the gamma-secretase catalytic subunit PSEN-1 in SMCs is an attractive potential therapeutic strategy for patients with SVAS/WBS that warrants further investigation.

Limitations of the study

An important limitation is that mechanistic links between elastin deficiency and upregulated PSEN-1 and -2 are not evaluated in this study. Our prior study reported that elastin deficiency reduces DNA methylation on promoters of *PSEN-1* and *-2* and increases their expression in human

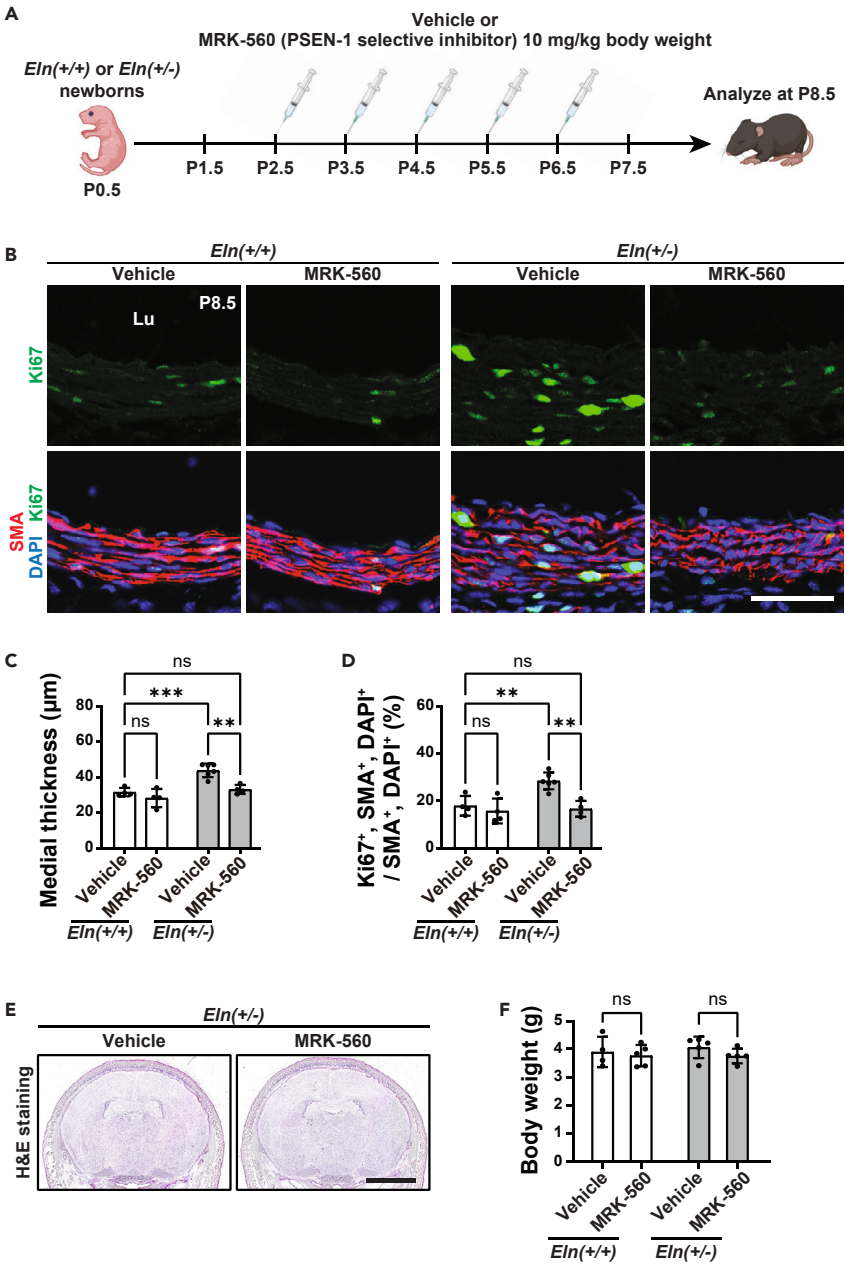

Figure 6. Postnatal MRK-560 treatment mitigates pre-established aortic muscularization in *Eln(+/–)* pups

Eln(+/+) or *Eln(+/–)* pups were injected daily with either vehicle or MRK-560 from P2.5–6.5 and collected at P8.5.

(A) Schematic of experimental schedule.

(B) Transverse aortic sections were stained for markers of Ki67, SMA, and DAPI.

(C) Histograms represent aortic medial wall thickness from sections at P8.5 as shown in B. n = 4–6 mice.

(D) Percent of SMCs that are $Ki67^+$ from sections represented in B. n = 4–6 mice.

(E) Brain coronal sections from *Eln(+/–)* pups with indicated treatment at P8.5 were subjected to H&E staining.

(F) Histograms represent body weight of each genotype and/or treatment. n = 4–5 mice. ns, not significant. $^{**}p < 0.01$, $^{***}p < 0.001$ by multifactor ANOVA with Tukey's *post hoc* test. Data are presented as mean ± SD. Scale bars, 50 μm (B) and 3 mm (E).

aortic SMCs in culture[18]; however, the regulatory mechanisms of DNA methylation in elastin aortopathy are not yet elucidated. A further limitation is the short-term follow-up of neonates with *Psen1* deletion in SMCs or pharmacological PSEN-1 inhibition. As loss of PSEN-1 in excitatory neuron induces progressive memory impairment and age-dependent neurodegeneration in adult mice,[22] future work assessing long-term neurodevelopment in neonates is important.

STAR★METHODS

Detailed methods are provided in the online version of this paper and include the following:

- KEY RESOURCES TABLE
- RESOURCE AVAILABILITY
  - Lead contact
  - Materials availability
  - Data and code availability
- EXPERIMENTAL MODEL AND STUDY PARTICIPANT DETAILS
  - Mice
  - Cell culture
- METHOD DETAILS
  - Immunohistochemistry
  - Quantification of aortic morphology
  - Mean linear intercept
  - Silencing of *ELN*
  - qRT-PCR
  - Western blot
  - *Psen1* deletion efficiency
  - Imaging
  - Vascular casting
  - Echocardiography
- QUANTIFICATION AND STATISTICAL ANALYSIS

SUPPLEMENTAL INFORMATION

Supplemental information can be found online at https://doi.org/10.1016/j.isci.2023.108636.

ACKNOWLEDGMENTS

We thank Dr. Jie Shen at Harvard Medical School for providing *Psen1(flox/flox)* mice and *Psen1(flox/flox), Psen2(−/−)* mice and Nicole Guerrera at Yale University School of Medicine for performing echocardiography. We are grateful to Greif laboratory members for their input. Junichi Saito was supported by the JSPS Overseas Research Fellowship from the Japan Society for the Promotion of Science (no. 202260284) and the AHA/CHF Congenital Heart Defect Research Award from the American Heart Association and the Children's Heart Foundation (23POSTCHF1022933). Funding was also provided by the National Institutes of Health (R01HD110059, R35HL150766, R21AG062202, R21NS123469 to D.M.G.), and American Heart Association (Established Investigator Award, 19EIA34660321 to D.M.G.).

AUTHOR CONTRIBUTIONS

J.S., J.M.D., and D.M.G. conceived of and designed experiments. J.S. and F.D.L performed them. J.S. and D.M.G. analyzed the results, prepared the figures, and wrote the article. All authors reviewed and provided input on the article.

DECLARATION OF INTERESTS

The authors declare no competing interests.

Received: June 16, 2023
Revised: November 16, 2023
Accepted: December 1, 2023
Published: December 13, 2023

REFERENCES

1. Sandberg, L.B., Soskel, N.T., and Leslie, J.G. (1981). Elastin structure, biosynthesis, and relation to disease states. N. Engl. J. Med. *304*, 566–579.
2. Karnik, S.K., Brooke, B.S., Bayes-Genis, A., Sorensen, L., Wythe, J.D., Schwartz, R.S., Keating, M.T., and Li, D.Y. (2003). A critical role for elastin signaling in vascular morphogenesis and disease. Development *130*, 411–423.
3. Brooke, B.S., Bayes-Genis, A., and Li, D.Y. (2003). New insights into elastin and vascular disease. Trends Cardiovasc. Med. *13*, 176–181.
4. Seidelmann, S.B., Lighthouse, J.K., and Greif, D.M. (2014). Development and pathologies of the arterial wall. Cell. Mol. Life Sci. *71*, 1977–1999.
5. Raines, E.W., and Ross, R. (1993). Smooth muscle cells and the pathogenesis of the lesions of atherosclerosis. Br. Heart J. *69*, S30–S37.
6. Li, D.Y., Brooke, B., Davis, E.C., Mecham, R.P., Sorensen, L.K., Boak, B.B., Eichwald, E., and Keating, M.T. (1998). Elastin is an essential determinant of arterial morphogenesis. Nature *393*, 276–280.
7. Curran, M.E., Atkinson, D.L., Ewart, A.K., Morris, C.A., Leppert, M.F., and Keating, M.T.

(1993). The elastin gene is disrupted by a translocation associated with supravalvular aortic stenosis. Cell *73*, 159–168.
8. Duque Lasio, M.L., and Kozel, B.A. (2018). Elastin-driven genetic diseases. Matrix Biol. *71–72*, 144–160.
9. Pober, B.R. (2010). Williams-Beuren syndrome. N. Engl. J. Med. *362*, 239–252.
10. Kozel, B.A., Barak, B., Kim, C.A., Mervis, C.B., Osborne, L.R., Porter, M., and Pober, B.R. (2021). Williams syndrome. Nat. Rev. Dis. Primers *7*, 42.
11. Li, D.Y., Faury, G., Taylor, D.G., Davis, E.C., Boyle, W.A., Mecham, R.P., Stenzel, P., Boak, B., and Keating, M.T. (1998). Novel arterial pathology in mice and humans hemizygous for elastin. J. Clin. Invest. *102*, 1783–1787.
12. Wagenseil, J.E., Ciliberto, C.H., Knutsen, R.H., Levy, M.A., Kovacs, A., and Mecham, R.P. (2009). Reduced vessel elasticity alters cardiovascular structure and function in newborn mice. Circ. Res. *104*, 1217–1224.
13. Deo, S.V., Burkhart, H.M., Dearani, J.A., and Schaff, H.V. (2013). Supravalvar aortic stenosis: current surgical approaches and outcomes. Expert Rev. Cardiovasc Ther. *11*, 879–890.
14. Baeten, J.T., and Lilly, B. (2017). Notch Signaling in Vascular Smooth Muscle Cells. Adv. Pharmacol. *78*, 351–382.
15. Mack, J.J., and Iruela-Arispe, M.L. (2018). NOTCH regulation of the endothelial cell phenotype. Curr. Opin. Hematol. *25*, 212–218.
16. Tetzlaff, F., and Fischer, A. (2018). Control of Blood Vessel Formation by Notch Signaling. Adv. Exp. Med. Biol. *1066*, 319–338.
17. Wang, T., Baron, M., and Trump, D. (2008). An overview of Notch3 function in vascular smooth muscle cells. Prog. Biophys. Mol. Biol. *96*, 499–509.
18. Dave, J.M., Chakraborty, R., Ntokou, A., Saito, J., Saddouk, F.Z., Feng, Z., Misra, A., Tellides, G., Riemer, R.K., Urban, Z., et al. (2022). JAGGED1/NOTCH3 activation promotes aortic hypermuscularization and stenosis in elastin deficiency. J. Clin. Invest. *132*.
19. Kimberly, W.T., LaVoie, M.J., Ostaszewski, B.L., Ye, W., Wolfe, M.S., and Selkoe, D.J. (2003). Gamma-secretase is a membrane protein complex comprised of presenilin, nicastrin, Aph-1, and Pen-2. Proc. Natl. Acad. Sci. USA *100*, 6382–6387.
20. Bergmans, B.A., and De Strooper, B. (2010). gamma-secretases: from cell biology to therapeutic strategies. Lancet Neurol. *9*, 215–226.
21. De Strooper, B. (2007). Loss-of-function presenilin mutations in Alzheimer disease. Talking Point on the role of presenilin mutations in Alzheimer disease. EMBO Rep. *8*, 141–146.
22. Yu, H., Saura, C.A., Choi, S.Y., Sun, L.D., Yang, X., Handler, M., Kawarabayashi, T., Younkin, L., Fedeles, B., Wilson, M.A., et al. (2001). APP processing and synaptic plasticity in presenilin-1 conditional knockout mice. Neuron *31*, 713–726.
23. Herreman, A., Hartmann, D., Annaert, W., Saftig, P., Craessaerts, K., Serneels, L., Umans, L., Schrijvers, V., Checler, F., Vanderstichele, H., et al. (1999). Presenilin 2 deficiency causes a mild pulmonary phenotype and no changes in amyloid precursor protein processing but enhances the embryonic lethal phenotype of presenilin 1 deficiency. Proc. Natl. Acad. Sci. USA *96*, 11872–11877.
24. Watanabe, H., Iqbal, M., Zheng, J., Wines-Samuelson, M., and Shen, J. (2014). Partial loss of presenilin impairs age-dependent neuronal survival in the cerebral cortex. J. Neurosci. *34*, 15912–15922.
25. Saura, C.A., Choi, S.Y., Beglopoulos, V., Malkani, S., Zhang, D., Shankaranarayana Rao, B.S., Chattarji, S., Kelleher, R.J., 3rd, Kandel, E.R., Duff, K., et al. (2004). Loss of presenilin function causes impairments of memory and synaptic plasticity followed by age-dependent neurodegeneration. Neuron *42*, 23–36.
26. Sen, S., Hallee, L., and Lam, C.K. (2021). The Potential of Gamma Secretase as a Therapeutic Target for Cardiac Diseases. J. Pers. Med. *11*.
27. Shen, J., Bronson, R.T., Chen, D.F., Xia, W., Selkoe, D.J., and Tonegawa, S. (1997). Skeletal and CNS defects in Presenilin-1-deficient mice. Cell *89*, 629–639.
28. Nakajima, M., Moriizumi, E., Koseki, H., and Shirasawa, T. (2004). Presenilin 1 is essential for cardiac morphogenesis. Dev. Dyn. *230*, 795–799.
29. Donoviel, D.B., Hadjantonakis, A.K., Ikeda, M., Zheng, H., Hyslop, P.S., and Bernstein, A. (1999). Mice lacking both presenilin genes exhibit early embryonic patterning defects. Genes Dev. *13*, 2801–2810.
30. Rivera-Torres, J., Guzman-Martinez, G., Villa-Bellosta, R., Orbe, J., Gonzalez-Gomez, C., Serrano, M., Diez, J., Andres, V., and Maraver, A. (2015). Targeting gamma-secretases protect against angiotensin II-induced cardiac hypertrophy. J. Hypertens. *33*, 843–850. discussion 850.
31. Misra, A., Sheikh, A.Q., Kumar, A., Luo, J., Zhang, J., Hinton, R.B., Smoot, L., Kaplan, P., Urban, Z., Qyang, Y., et al. (2016). Integrin beta3 inhibition is a therapeutic strategy for supravalvular aortic stenosis. J. Exp. Med. *213*, 451–463.
32. Salvador, J., Hernandez, G.E., Ma, F., Abrahamson, C.W., Pellegrini, M., Goldman, R., Ridge, K.M., and Iruela-Arispe, M.L. (2022). Transcriptional Evaluation of the Ductus Arteriosus at the Single-Cell Level Uncovers a Requirement for Vim (Vimentin) for Complete Closure. Arterioscler. Thromb. Vasc. Biol. *42*, 732–742.
33. Staiculescu, M.C., Cocciolone, A.J., Procknow, J.D., Kim, J., and Wagenseil, J.E. (2018). Comparative gene array analyses of severe elastic fiber defects in late embryonic and newborn mouse aorta. Physiol Genomics *50*, 988–1001.
34. Jiao, Y., Li, G., Korneva, A., Caulk, A.W., Qin, L., Bersi, M.R., Li, Q., Li, W., Mecham, R.P., Humphrey, J.D., and Tellides, G. (2017). Deficient Circumferential Growth Is the Primary Determinant of Aortic Obstruction Attributable to Partial Elastin Deficiency. Arterioscler. Thromb. Vasc. Biol. *37*, 930–941.
35. Lin, C.J., Hunkins, B.M., Roth, R.A., Lin, C.Y., Wagenseil, J.E., and Mecham, R.P. (2021). Vascular Smooth Muscle Cell Subpopulations and Neointimal Formation in Mouse Models of Elastin Insufficiency. Arterioscler. Thromb. Vasc. Biol. *41*, 2890–2905.
36. Mecham, R.P. (2018). Elastin in lung development and disease pathogenesis. Matrix Biol. *73*, 6–20.
37. Wendel, D.P., Taylor, D.G., Albertine, K.H., Keating, M.T., and Li, D.Y. (2000). Impaired distal airway development in mice lacking elastin. Am. J. Respir. Cell Mol. Biol. *23*, 320–326.
38. Shifren, A., Durmowicz, A.G., Knutsen, R.H., Hirano, E., and Mecham, R.P. (2007). Elastin protein levels are a vital modifier affecting normal lung development and susceptibility to emphysema. Am. J. Physiol. Lung Cell Mol. Physiol. *292*, L778–L787.
39. Borgegard, T., Gustavsson, S., Nilsson, C., Parpal, S., Klintenberg, R., Berg, A.L., Rosqvist, S., Serneels, L., Svensson, S., Olsson, F., et al. (2012). Alzheimer's disease: presenilin 2-sparing gamma-secretase inhibition is a tolerable Abeta peptide-lowering strategy. J. Neurosci. *32*, 17297–17305.
40. Lee, M.K., Slunt, H.H., Martin, L.J., Thinakaran, G., Kim, G., Gandy, S.E., Seeger, M., Koo, E., Price, D.L., and Sisodia, S.S. (1996). Expression of presenilin 1 and 2 (PS1 and PS2) in human and murine tissues. J. Neurosci. *16*, 7513–7525.
41. Rogaev, E.I., Sherrington, R., Rogaeva, E.A., Levesque, G., Ikeda, M., Liang, Y., Chi, H., Lin, C., Holman, K., Tsuda, T., et al. (1995). Familial Alzheimer's disease in kindreds with missense mutations in a gene on chromosome 1 related to the Alzheimer's disease type 3 gene. Nature *376*, 775–778.
42. Levy-Lahad, E., Wasco, W., Poorkaj, P., Romano, D.M., Oshima, J., Pettingell, W.H., Yu, C.E., Jondro, P.D., Schmidt, S.D., Wang, K., et al. (1995). Candidate gene for the chromosome 1 familial Alzheimer's disease locus. Science *269*, 973–977.
43. Sannerud, R., Esselens, C., Ejsmont, P., Mattera, R., Rochin, L., Tharkeshwar, A.K., De Baets, G., De Wever, V., Habets, R., Baert, V., et al. (2016). Restricted Location of PSEN2/gamma-Secretase Determines Substrate Specificity and Generates an Intracellular Abeta Pool. Cell *166*, 193–208.
44. Zhang, Z., Nadeau, P., Song, W., Donoviel, D., Yuan, M., Bernstein, A., and Yankner, B.A. (2000). Presenilins are required for gamma-secretase cleavage of beta-APP and transmembrane cleavage of Notch-1. Nat. Cell Biol. *2*, 463–465.
45. McCaw, T.R., Inga, E., Chen, H., Jaskula-Sztul, R., Dudeja, V., Bibb, J.A., Ren, B., and Rose, J.B. (2021). Gamma Secretase Inhibitors in Cancer: A Current Perspective on Clinical Performance. Oncologist *26*, e608–e621.
46. Collins, M., Michot, J.M., Bellanger, C., Mussini, C., Benhadji, K., Massard, C., and Carbonnel, F. (2021). Notch inhibitors induce diarrhea, hypercrinia and secretory cell metaplasia in the human colon. EXCLI J *20*, 819–827.
47. van Es, J.H., van Gijn, M.E., Riccio, O., van den Born, M., Vooijs, M., Begthel, H., Cozijnsen, M., Robine, S., Winton, D.J., Radtke, F., and Clevers, H. (2005). Notch/gamma-secretase inhibition turns proliferative cells in intestinal crypts and adenomas into goblet cells. Nature *435*, 959–963.
48. Doody, R.S., Raman, R., Farlow, M., Iwatsubo, T., Vellas, B., Joffe, S., Kieburtz, K., He, F., Sun, X., Thomas, R.G., et al. (2013). A phase 3 trial of semagacestat for treatment of Alzheimer's disease. N. Engl. J. Med. *369*, 341–350.
49. Doerfler, P., Shearman, M.S., and Perlmutter, R.M. (2001). Presenilin-dependent gamma-secretase activity modulates thymocyte development. Proc. Natl. Acad. Sci. USA *98*, 9312–9317.
50. Wong, G.T., Manfra, D., Poulet, F.M., Zhang, Q., Josien, H., Bara, T., Engstrom, L., Pinzon-Ortiz, M., Fine, J.S., Lee, H.J., et al. (2004). Chronic treatment with the gamma-secretase

inhibitor LY-411,575 inhibits beta-amyloid peptide production and alters lymphopoiesis and intestinal cell differentiation. J. Biol. Chem. *279*, 12876–12882.

51. de Vera Mudry, M.C., Regenass-Lechner, F., Ozmen, L., Altmann, B., Festag, M., Singer, T., Muller, L., Jacobsen, H., and Flohr, A. (2012). Morphologic and functional effects of gamma secretase inhibition on splenic marginal zone B cells. Int. J. Alzheimer's Dis. 289412.
52. Escamilla-Ayala, A., Wouters, R., Sannerud, R., and Annaert, W. (2020). Contribution of the Presenilins in the cell biology, structure and function of gamma-secretase. Semin. Cell Dev. Biol. *105*, 12–26.
53. Habets, R.A., de Bock, C.E., Serneels, L., Lodewijckx, I., Verbeke, D., Nittner, D., Narlawar, R., Demeyer, S., Dooley, J., Liston, A., et al. (2019). Safe targeting of T cell acute lymphoblastic leukemia by pathology-specific NOTCH inhibition. Sci. Transl. Med. *11*.
54. Guner, G., and Lichtenthaler, S.F. (2020). The substrate repertoire of gamma-secretase/presenilin. Semin. Cell Dev. Biol. *105*, 27–42.
55. Cai, J., Chen, Z., Ruan, Q., Han, S., Liu, L., Qi, X., Boye, S.L., Hauswirth, W.W., Grant, M.B., and Boulton, M.E. (2011). gamma-Secretase and presenilin mediate cleavage and phosphorylation of vascular endothelial growth factor receptor-1. J. Biol. Chem. *286*, 42514–42523.
56. Boulton, M.E., Cai, J., and Grant, M.B. (2008). gamma-Secretase: a multifaceted regulator of angiogenesis. J. Cell Mol. Med. *12*, 781–795.
57. Ni, C.Y., Murphy, M.P., Golde, T.E., and Carpenter, G. (2001). gamma -Secretase cleavage and nuclear localization of ErbB-4 receptor tyrosine kinase. Science *294*, 2179–2181.
58. McElroy, B., Powell, J.C., and McCarthy, J.V. (2007). The insulin-like growth factor 1 (IGF-1) receptor is a substrate for gamma-secretase-mediated intramembrane proteolysis. Biochem. Biophys. Res. Commun. *358*, 1136–1141.
59. Lilly, B. (2014). We have contact: endothelial cell-smooth muscle cell interactions. Physiology *29*, 234–241.
60. Hirata, N., Yamada, S., Shoda, T., Kurihara, M., Sekino, Y., and Kanda, Y. (2014). Sphingosine-1-phosphate promotes expansion of cancer stem cells via S1PR3 by a ligand-independent Notch activation. Nat. Commun. *5*, 4806.
61. Gridley, T. (2007). Notch signaling in vascular development and physiology. Development *134*, 2709–2718.
62. Fang, J.S., Dai, C., Kurjiaka, D.T., Burt, J.M., and Hirschi, K.K. (2013). Connexin45 regulates endothelial-induced mesenchymal cell differentiation toward a mural cell phenotype. Arterioscler. Thromb. Vasc. Biol. *33*, 362–368.
63. Hirschi, K.K., Burt, J.M., Hirschi, K.D., and Dai, C. (2003). Gap junction communication mediates transforming growth factor-beta activation and endothelial-induced mural cell differentiation. Circ. Res. *93*, 429–437.
64. Sawada, H., Rateri, D.L., Moorleghen, J.J., Majesky, M.W., and Daugherty, A. (2017). Smooth Muscle Cells Derived From Second Heart Field and Cardiac Neural Crest Reside in Spatially Distinct Domains in the Media of the Ascending Aorta-Brief Report. Arterioscler. Thromb. Vasc. Biol. *37*, 1722–1726.
65. Li, X., Zhang, X., Leathers, R., Makino, A., Huang, C., Parsa, P., Macias, J., Yuan, J.X., Jamieson, S.W., and Thistlethwaite, P.A. (2009). Notch3 signaling promotes the development of pulmonary arterial hypertension. Nat Med *15*, 1289–1297.
66. Shifren, A., Durmowicz, A.G., Knutsen, R.H., Faury, G., and Mecham, R.P. (2008). Elastin insufficiency predisposes to elevated pulmonary circulatory pressures through changes in elastic artery structure. J. Appl. Physiol. *105*, 1610–1619.
67. Sugitani, H., Hirano, E., Knutsen, R.H., Shifren, A., Wagenseil, J.E., Ciliberto, C., Kozel, B.A., Urban, Z., Davis, E.C., Broekelmann, T.J., and Mecham, R.P. (2012). Alternative splicing and tissue-specific elastin misassembly act as biological modifiers of human elastin gene frameshift mutations associated with dominant cutis laxa. J. Biol. Chem. *287*, 22055–22067.
68. Hirano, E., Knutsen, R.H., Sugitani, H., Ciliberto, C.H., and Mecham, R.P. (2007). Functional rescue of elastin insufficiency in mice by the human elastin gene: implications for mouse models of human disease. Circ. Res. *101*, 523–531.
69. Wendling, O., Bornert, J.M., Chambon, P., and Metzger, D. (2009). Efficient temporally-controlled targeted mutagenesis in smooth muscle cells of the adult mouse. Genesis *47*, 14–18.
70. Wang, Y., Nakayama, M., Pitulescu, M.E., Schmidt, T.S., Bochenek, M.L., Sakakibara, A., Adams, S., Davy, A., Deutsch, U., Luthi, U., et al. (2010). Ephrin-B2 controls VEGF-induced angiogenesis and lymphangiogenesis. Nature *465*, 483–486.
71. Yu, H., Kessler, J., and Shen, J. (2000). Heterogeneous populations of ES cells in the generation of a floxed Presenilin-1 allele. Genesis *26*, 5–8.
72. Steiner, H., Duff, K., Capell, A., Romig, H., Grim, M.G., Lincoln, S., Hardy, J., Yu, X., Picciano, M., Fechteler, K., et al. (1999). A loss of function mutation of presenilin-2 interferes with amyloid beta-peptide production and notch signaling. J. Biol. Chem. *274*, 28669–28673.
73. Liu, Z., Fu, S., and Tang, N. (2017). A Standardized Method for Measuring Internal Lung Surface Area via Mouse Pneumonectomy and Prosthesis Implantation. J. Vis. Exp. 56114.

STAR★METHODS

KEY RESOURCES TABLE

REAGENT or RESOURCE	SOURCE	IDENTIFIER
Antibodies		
Rabbit anti-PSEN-1	Cell Signaling Technology	Cat# 5643; RRID:AB_10706356
Rabbit anti-PSEN-2	Cell Signaling Technology	Cat# 9979; RRID:AB_10829910
Rabbit anti-HES1	Cell Signaling Technology	Cat# 11988; RRID:AB_2728766
Rabbit anti-HEY1	Abcam	Cat# ab235173; RRID: AB_3076433
Rabbit anti-NOTCH3	Abcam	Cat# ab23426; RRID:AB_776841
Rabbit anti-Ki67	Invitrogen	Cat# MA5-14520; RRID:AB_10979488
Rat anti-CD31	BD Pharmingen	Cat# 553370; RRID:AB_394816
Rabbit anti-COL I	Novus Biologicals	Cat# NB600-408; RRID:AB_10000511
Rabbit anti-COL IV	Abcam	Cat# ab19808; RRID:AB_445160
Rabbit anti-COL VI	Abcam	Cat# ab182744; RRID:AB_2847919
Rabbit anti-COL VIII	Proteintech	Cat# 17251-1-AP; RRID:AB_10696173
Conjugated Cy3 mouse anti-SMA	Sigma-Aldrich	Cat# C6198; RRID:AB_476856
Rabbit anti-GAPDH	Cell Signaling Technology	Cat# 2118; RRID:AB_561053
Rabbit anti-ELN	Dave et al.[18]; Shifren et al.[66]; Sugitani et al.[67]; Hirano et al.[68]	MRT6-17
Chemicals, peptides, and recombinant proteins		
Tamoxifen	Sigma-Aldrich	T5648
Progesterone	Sigma-Aldrich	P3972
MRK-560	Sigma-Aldrich	SML3330
Recombinant Human EGF	PeproTech	AF-100-15
Recombinant Human FGF	PeproTech	AF-100-18B
Experimental models: Cell lines		
Human Aortic Smooth Muscle Cells	Lonza	CC-2571
Experimental models: Organisms/strains		
C57BL/6 mice	The Jackson Laboratory	JAX: 000664
Eln(+/−) mice	Dr. Dean Li	MGI: 2153007
Acta2-CreER^{T2} mice	Drs. Pierre Chambon and Daniel Metzger	MGI: 3831911
Cdh5-CreER^{T2} mice	Dr. Ralf Adams (via Dr. Michael Simons)	MGI:3848982
Psen1(flox/flox) mice	Dr. Jie Shen	JAX: 004825
Psen2(−/−) mice	Dr. Jie Shen	MGI: 2664242
Oligonucleotides		
siRNA targeting human ELN	Horizon Discovery Biosciences Limited	L-009306-00
Non-targeting siRNA	Horizon Discovery Biosciences Limited	D-001810-10
Primer sequences used for genotyping	See Table S1	
Primer pair sequences used for quantitative reverse transcription polymerase chain reactions	See Table S2	
Software and algorithms		
ImageJ	NIH	https://ImageJ.net/ij/index.html
GraphPad Prism (version 9.4.1)	GraphPad	https://www.graphpad.com/scientific-software/prism/

(*Continued on next page*)

Continued

REAGENT or RESOURCE	SOURCE	IDENTIFIER
Other		
gentleMACS C Tubes	Miltenyi Biotec	130-093-237
Lung Dissociation Kit, mouse	Miltenyi Biotec	130-095-927
gentleMACS Dissociator	Miltenyi Biotec	130-093-235
Dynabeads Sheep Anti-Rat IgG	Invitrogen	11035

RESOURCE AVAILABILITY

Lead contact

Further information and requests for resources and reagents should be directed to and will be fulfilled by the lead contact, Daniel Greif (daniel.greif@yale.edu).

Materials availability

This study did not generate new unique reagents.

Data and code availability

(1) All data reported in this paper will be shared by the lead contact upon request.
(2) This paper does not report original code.
(3) Any additional information required to reanalyze the data reported in this paper is available from the lead contact upon request.

EXPERIMENTAL MODEL AND STUDY PARTICIPANT DETAILS

Mice

C57BL/6 WT mice were from The Jackson Laboratory. Mouse strains used were *Eln(+/–)*,[6] *Acta2-CreER^{T2}*,[69] *Cdh5-CreER^{T2}*,[70] *Psen1(flox/flox)*,[71] and *Psen2(–/–)*.[72] Primer sequences used for genotyping are provided in Table S1. Mice were bred and pups were harvested after birth. E0.5 was considered the time of vaginal plug. For genetic deletion using *Psen1(flox/flox)* allele, we administered 1 mg tamoxifen (Sigma-Aldrich, T5648) with concomitant 0.25 mg progesterone (Sigma-Aldrich, P3972) intraperitoneally to pregnant dams on E14.5 and E15.5, and analyzed pups immediately after birth. For pharmacological inhibition of PSEN-1, pregnant dams were intraperitoneally injected with either MRK-560 (30 mg/kg body weight, Sigma-Aldrich, SML3330)[53] or vehicle (10% DMSO in corn oil) on either E14.5 and E15.5 or on E16.5 and E17.5, and pups were analyzed at P0.5. For postnatal administration of MRK-560, *Eln(+/+)* or *Eln(+/–)* mice were injected daily with either MRK-560 (10 mg/kg body weight) or vehicle (0.4% DMSO in corn oil) from P2.5–6.5, and analyzed at P8.5. Our previous study did not detect sex-dependent differences in elastin mutant mice,[18] and thus, this study analyzed both sexes. All mouse experiments were approved by the Institutional Animal Care and Use Committee at Yale University and in accordance with the NIH *Guide for the Care and Use of Laboratory Animals* (National Academies Press, 2011).

Cell culture

Human aortic SMCs were obtained from Lonza (CC-2571). The SMCs were cultured up to passage 6 in M199 medium supplemented with 10% FBS and growth factors (PeproTech, EGF and FGF).

METHOD DETAILS

Immunohistochemistry

After euthanasia, pups were fixed in 4% paraformaldehyde for 2 h. These samples were then washed with PBS for 2 h and incubated with 30% sucrose in PBS for 24–48 h at 4°C until the sample sunk. Samples were embedded in OCT compound (Tissue-Tek), frozen on dry ice, and stored at −80°C. Transverse serial cryosections of ascending aortas were cut 8 μm thick starting immediately below the aortic arch and proceeding caudally, ending at the aortic valve. As described in the main text, cranial, caudal, and middle position of ascending aortas were analyzed in Figure S2. All other experiments were performed at the cranial position, which is in proximity to the aortic arch. For immunostaining, cryosections were washed with 0.5% Tween 20 in PBS (PBS-T) and incubated with blocking solution (5% goat serum, 0.1% Triton X-100 in PBS) for 1 h. Then, the sections were incubated with primary antibodies diluted in blocking solution overnight at 4°C. On the next day, sections were washed with PBS-T and incubated with secondary antibodies diluted in blocking solution for 1 h. Primary antibodies were rabbit anti-PSEN-1 (Cell Signaling Technology, 5643; 1:150), rabbit anti-PSEN-2 (Cell Signaling Technology, 9979; 1:250), rabbit anti-HES1 (Cell Signaling Technology, 11988; 1:1000), rabbit anti-HEY1 (Abcam, ab235173; 1:200), rabbit anti-NOTCH3 (Abcam, ab23426; 1:200), rabbit anti-Ki67 (Invitrogen, MA5-14520; 1:250), rat anti-CD31 (BD Pharmingen, 553370; 1:150), rabbit anti-COL I (Novus Biologicals, NB600-408; 1:200), rabbit

anti-COL IV (Abcam, ab19808; 1:200), rabbit anti-COL VI (Abcam, ab182744; 1:200), rabbit anti-COL VIII (Proteintech, 17251-1-AP; 1:200) and directly conjugated Cy3 mouse anti-SMA (Sigma-Aldrich, C6198; 1:500). Secondary antibodies against rabbit or rat were conjugated to Alexa Fluor 488 or 647 (Molecular Probes, 1:500). DAPI (Sigma-Aldrich, D9542; 1:300) was used for nuclear staining.

Quantification of aortic morphology

ImageJ software (NIH) was used for quantifications. Transverse sections were used for aortic medial wall and lumen qualifications. The medial wall thickness from transverse sections of murine aorta were calculated by measuring the distance between the inner aspect of the inner and the outer aspect of the outer SMA^+ medial layers.[18] Medial and lumen areas were calculated by measuring the area of SMA staining and the area interior to CD31 staining, respectively.[18]

Mean linear intercept

Mean linear intercept was used for assessment of lung emphysema.[73] Lungs from pups with each genotype and/or treatment were subjected to H&E staining and images were collected using a 10× objective for 3 sections per lung. A grid with 5 lines of finite length (500 μm) was placed over each image. The value of one intercept was defined as the linear length between two adjacent alveolar epithelia. For each line, the values of all intercepts were quantified. A larger value represents more simplified alveoli.

Silencing of *ELN*

Human aortic SMCs were transfected with Lipofectamine 2000 (Life Technologies) containing siRNA targeted against *ELN* (Horizon Discovery Biosciences Limited, 50 nM) or Scr RNA for 6 h.[18] Cells were then washed in M199 medium and cultured for 72 h prior to collection for qRT-PCR or Western blot analysis.[18]

qRT-PCR

For pups at P0.5, the entire aorta from the root to the iliac arteries was dissected and was homogenized with tissue homogenizer (Wheaton) in lysis buffer (ThermoFisher). RNA was isolated from mouse aortas and human aortic SMCs with the PureLink RNA Mini Kit (ThermoFisher). Isolated RNA was reverse transcribed with the iScript cDNA Synthesis Kit (Bio-Rad). cDNA was subjected to qRT-PCR on a CFX96 Real-Time System (Bio-Rad) using SsoFast Eva-Green supermix (Bio-Rad) and primers as shown in Table S2 mRNA levels were normalized relative to 18S rRNA for cultured cells and to 18S rRNA or Gapdh for murine samples.

Western blot

For protein analysis, aortas from pups were mechanically lysed in RIPA buffer with protease and phosphatase inhibitor cocktails (ThermoFisher) on ice with a glass pestle tissue homogenizer (Pyrex). Cultured human aortic SMCs were also collected in RIPA buffer and vortexed every 10 min for 1 h on ice. Lysates were then centrifuged at 13,000g, 4°C for 5 min and supernatants were collected. BCA assay (ThermoFisher) was used to determine the protein concentration. Lysates were prepared in 4× Laemmli sample buffer (Bio-Rad) at 95°C for 5 min. Protein samples with Laemmli buffer were resolved by 4–20% SDS-PAGE, transferred to Immobilon PVDF membranes (Millipore), blocked with 5% nonfat dry milk or bovine serum albumin in TBS with tween 20 (TBS-T), washed in TBS-T, and incubated with primary antibodies diluted in blocking solution overnight at 4°C. On the next day, membranes were washed in TBS-T, incubated with HRP-conjugated secondary antibodies (Dako), washed in TBS-T again, and developed with Supersignal West Femto Maximum Sensitivity Substrate (ThermoFisher) on the G:BOX imaging system (Syngene). Western blot analysis used primary antibodies raised in rabbits and targeting PSEN-1 (Cell Signaling Technology, 5643; 1:1000), PSEN-2 (Cell Signaling Technology, 9979; 1:1000), GAPDH (Cell Signaling Technology, 2118; 1:2500), and ELN (raised against exons 6–17 of recombinant mouse tropoelastin; 1:500).[18,66–68]

Psen1 deletion efficiency

To elucidate *Psen1* deletion efficiency with *Acta2-CreER^{T2}*, pregnant dams bearing *Psen1(flox/flox)* embryos with no Cre or *Acta2-CreER^{T2}* were injected with tamoxifen at E14.5 and E15.5, and pups were collected at P0.5.[18] Aortas were dissected and the adventitial layer was carefully removed. The remaining medial layer was collected in lysis buffer (ThermoFisher) and mechanically homogenized with a glass pestle tissue homogenizer. RNA was purified for qRT-PCR, and protein was prepared for Western blot as described above. For genotyping, genomic DNA was extracted from the aortic media by incubation with 50 mM NaOH at 95°C for 1 h, and then 100 mM Tris-HCl pH 7.5 was added to neutralize the digested samples. After centrifugation at 13,000g for 5 min, supernatants were used for genotyping PCR with primers as shown in Table S1.

To determine *Psen1* deletion efficiency with *Cdh5-CreER^{T2}*, pregnant dams bearing *Psen1(flox/flox)* embryos with or without *Cdh5-CreER^{T2}* were injected with tamoxifen at E14.5 and E15.5, and pups were collected at P0.5. Dissected lungs from pups were transferred to gentleMACS C Tubes (130-093-237, Miltenyi) containing 5 mL dissociation enzyme (130-095-927, Miltenyi) and incubated at 37°C for 20 min.[18] Samples were then processed with the gentleMACS Dissociator (Miltenyi, 130-093-235) for further cell dissociation. The lung cell suspension was filtered with 70 μm strainer, and the enzyme reaction was stopped with 1 mL FBS. The resulting cell suspension was centrifuged at 500 rpm for 5 min, and the cell pellet was resuspended in M199 medium. Subsequently, magnetic beads (Invitrogen, 11035), which were pre-coated with

anti-mouse-CD31 antibody (BD Pharmingen, 553370), were added to the cell suspensions and together were incubated on a rotator for 20 min.[18] ECs bound to magnet beads were collected with a magnet stand and used for qRT-PCR, Western blot, and genotyping.

Imaging

Fluorescence images of aortic sections were acquired with a confocal microscope (PerkinElmer UltraView Vox Spinning Disc). Brightfield images of H&E staining were captured using a BX63 microscope (Olympus). Adobe Photoshop was used for image processing.

Vascular casting

After euthanization of pups with isoflurane, the chest wall was opened, and left leg was removed. PBS was injected in the left ventricle and blood was drained through the left iliac artery. Yellow latex (Ward's Science, 470024-616) was then injected through the left ventricle.[35] Mice were then kept moist at 4°C for 3-4 h to facilitate setting of the injected latex. Mice were subsequently fixed in 4% PFA at 4 °C overnight, followed by fine dissection to demonstrate aortic morphology.

Echocardiography

Transthoracic echocardiograms were performed on pups at P0.5 under light anesthesia (1.5–2% isoflurane) while maintaining physiological temperatures. Two-dimensional, m-mode, and pulsed wave Doppler images were obtained by a high-resolution ultrasound system (Vevo 2100, VisualSonics, Toronto, Ontario, Canada) equipped with an ultra-high frequency (40 MHz) linear array transducer.

QUANTIFICATION AND STATISTICAL ANALYSIS

Two-tailed Student's *t* test and multifactor ANOVA with Tukey's *post hoc* test were used to analyze data using GraphPad Prism (version 9.4.1). The number of mice per experiment are described in each figure legend. Statistical significance threshold was set at a p value less than 0.05. All data are presented as mean $\pm$ SD.